Entropy generation minimization of an advanced two-bed adsorption refrigeration system

S. Yagnamurthy[a], P. R. Chauhan[b], B. B. Saha[c], and S. K. Tyagi[b*]

[a] School of Engineering, The University of Warwick, Coventry CV47AL, United Kingdom

[b] Department of Energy Science and Engineering, Indian Institute of Technology Delhi, Hauz Khas, New Delhi 110016, India

[c] Mechanical Engineering Department, Kyushu University, 744 Motooka, Nishi-ku, Fukuoka 819-0395, Japan

Abstract

This article presents the thermodynamic assessment of an advanced adsorption chiller with an aim towards entropy generation minimization through the selection of appropriate operating strategies, temperatures, and design modifications. The present study carries out a second law analysis of a two-bed silica gel water pair-based adsorption cooling system, with a focus on the under-explored aspects of heat recovery strategy and auxiliary consumption reducing measures. A second law performance index *viz*. specific irreversibility is introduced for effectively incorporating the entropy generation, auxiliary electricity consumption and cooling capacity and it has been further verified to be an indicator of second law efficiency . The performance of the system has been numerically evaluated under the normal and passive heat recovery strategies, where it is found that the passive heat recovery strategy offers a lower entropy generation by 63%. The lowest specific irreversibility has been identified for a hot water inlet temperature of 65°C. The study further investigates the second law efficiency impact of adopting a capillary-assisted evaporator for auxiliary electricity consumption reduction. It is observed that the specific irreversibility could reduce by up to 22% over a conventional falling film design. The analysis and results presented in this study are anticipated to increase the effectiveness of adsorption chillers for heat recovery applications.

Keywords: adsorption chiller; capillary assisted evaporator; entropy generation; passive heat recovery; silica gel-water.

* Corresponding author: Email: sudhirtyagi@yahoo.com (S. K. Tyagi)

Nomenclature

A	Area of cross-section of mass transfer, (m^2)
ACS	Adsorption cooling system
C_p	Specific heat capacity, (kJ/kg-K)
COP	Coefficient of performance
d	Heterogeneity parameter
D_o	Preexponential constant, (m^2/s)
E_a	Activation energy, (kJ/kg)
h_{fg}	Enthalpy of vaporisation, (kJ/kg)
HR	Heat recovery
K_o	Pre exponential Toth's constant, (Pa^{-1})
LMTD	Logarithmic temperature difference
$\dot{m}$	Mass flow rate, (kg/s)
N	Number of segments
P	Pressure, (Pa)
Q_{st}	Heat of adsorption, (kJ/kg)
R	Gas constant, (kJ/kg.K)
R_p	Radius of adsorbent particle, (m)
S_{gen}	Entropy generation, (kW/kg-K)
T	Temperature, (K)
t	Time, (s)
x	Concentration of refrigerant, (kg/kg)
X	Specific irreversibility, (kJ/kJ)
x*	Saturation concentration of refrigerant, (kg/kg)
M	Mass, (kg)
UA	Heat transfer coefficient (kW/K)
φ	Time of commencement of switch-over phase, (s)
η	Second law efficiency parameter

Subscripts

ads	Adsorber
bed	Adsorbent bed
chill	Chilled water
cond	Condenser
cool	Cooling water
cyc	Cycle
des	Desorber
eq	Equilibrium
evap	Evaporator
hex	Heat exchanger
hot	Hot water
HT	Heat transfer
in	Inlet
MT	Mass transfer

out	Outlet	w	Water
tot	Total		

1. Introduction

In recent years, the adsorption technology-based cooling [1-4] and heating [5, 6] systems are gaining greater attention from researchers and scientists as a long-term sustainable technology option to fulfill the fast-growing cooling and refrigeration demands in the industry, small vehicles, offices, and buildings [7]. This is owing to its capability to produce the desired effect at the required temperature using non-payable, low-grade, abundantly available, ultra-low temperature [8, 9] thermal energy sources found in nature as well as in household applications. Adsorption cooling systems (ACSs), with the exception of the compression mechanism, are similar to conventional refrigeration systems (Vapour compression refrigeration system) in terms of working principles and operation processes [10]. However, the ineffective heat and mass transfer processes in the adsorption cooling cycle result in a low coefficient of performance (COP), a bulky system, and a lack of economic viability. Researchers have attempted to address these issues through the synthesis of highly microporous [11, 12] and granular adsorbent beds [13, 14] and the application of micro-scaled heat exchangers [15], coated adsorbers [16], etc. such as miniaturised heat and mass transfer devices. Along with the design improvements, attempts have been made for performance enhancement through various operational strategies such as heat and mass recovery [17], multistage [18], etc., and operating parameter optimization [19]. The ideal ACS consists of generally four types of equipment; the condenser, expansion valve, evaporator, and adsorber/desorber (thermal compressor) [20]. In reality, all the processes associated with each piece of equipment have some amount of irreversibility within the system [21]. The entropy generation occurring in a chiller can be associated with mass transfer, heat transfer, and flushing, resulting in the loss of the desired effect and hence diminishing the thermal performance of the ACS as compared to the ideal processes. In this regard, a second law-based thermodynamic analysis can be a useful tool to perceive the irreversibilities of various components of the chiller and their impact on thermal performance [22].

The idea of entropy generation and entropy generation number for heat and mass transfer is first introduced by Andrian Bejan to design the heat exchanger device [23].

From the published literature, several research attempts have been made by many researchers in terms of qualitative analysis (second law of thermodynamics) of ACS. Meunier et al. [24] performed a comparative theoretical investigation in terms of entropy generation for sorption refrigeration systems such as liquid absorption, solid adsorption, and chemical reaction heat pumps. It is then observed that the irreversibilities caused by thermal coupling are more responsible for degrading the coefficient of performance (COP) of adsorption-based cooling systems, while in the case of absorption cooling systems with solution heat exchangers, the internal irreversibility dominates for the same. Several researchers attempted to appropriately quantify the entropy generation to understand its impact on the system performance. Meunier et al. [25] studied the performance impact of the cycle time of an ACS using entropy production number estimation. They observed that longer external thermal entropy generation is significantly affected at longer cycle times, while internal thermal entropy generation is more significant at lower cycle times. A two-bed adsorption cooling cycle using entropic mean temperatures is investigated, which helped to identify the significance of thermal regeneration and the influence of cycle times and heat transfer fluid flow rates on the thermodynamic efficiency. Pons et al. (1996) analysed a two-bed adsorption cooling cycle using entropic mean temperatures, which helped to identify the significance of thermal regeneration and the influence of cycle times and heat transfer fluid flow rates on thermodynamic efficiency [26]. Meunier studied the impact of cascading several beds for a given set of heat reservoir temperatures and observed that the second law efficiency approaches 68% of the ideal Carnot COP with an infinite number of cascaded beds [27]. Pons [28] carried out entropy generation analysis for adsorption chillers and defined dimensionless parameters for entropy production quantification. The identification of the optimal operational parameters of an adsorption chiller was attempted based on a correlation fitting between the entropy production parameters. The second law analysis has helped researchers to identify the key components and processes affecting the system COP. Chua et al. [29] represented the batch-wise operating cycle of adsorption cooling systems using a time-invariant T-S diagram. They have identified it to be a useful tool for determining the energy contributions of various processes and studied the impact of varying operational parameters [30]. In another investigation, Chua et al. [31] identified the maximum entropy generation to be occurring in the beds with heat transfer being the bottle neck. They have further identified that the maximum contribution is

during the switch over phase. Myat et al. [32] incorporated a genetic algorithm along with an entropy generation minimization technique to trace the most favorable thermal performance of ACS using different sets of working parameters. The second law analysis has been further found to be useful in thermo-economic evaluations to assess the cost rate based on exergy destruction in adsorption systems [33].

From the literature review, it is inferred that most of the research efforts dealt with the assessment of entropy generation and optimization across various components of the chiller. However, the impact of performance enhancement strategies on entropy generation has not been studied in the literature as far as the knowledge of the authors is concerned. This requires a holistic assessment of entropy generation at the heat reservoirs viz., heat source and heat sink, along with that occurring at the ACS. Therefore, the present study attempts to estimate and address these aspects, through a second law-based analysis of a two-bed ACS under normal and a passive heat recovery operational modes. The ACS is of 10kW cooling capacity and employs silica gel-water pair [36]. The determination of entropy at the heat source and sink can be a crucial aspect in determining the effectiveness of adsorption cooling systems when employed for waste heat recovery applications. It is also observed that the impact of auxiliary power consumption within an ACS on the overall system irreversibility has been an under-explored area in the literature. This can be particularly useful to understand the impact of design improvements of various components on the second law efficiency. Capillary evaporators are one of such relatively recent developments in ACS, which are seen to eliminate the need for a circulation pump in the evaporator chamber and save auxiliary electric power consumption [37-41]. The present study attempts to explore the impact of a capillary-assisted evaporator design on the second law efficiency, over that of a falling film design. Specific irreversibility is evaluated as an indicator of the second law efficiency for incorporating the aspects of entropy generation, cooling capacity and auxiliary electricity consumption. To summarise, the objectives of the present study are:

i. Entropy generation evaluation across various components of the chiller under default operation mode.
ii. Entropy generation evaluation under passive heat recovery mode and specific irreversibility evaluation for the two operating modes.
iii. Specific irreversibility evaluation with a suitable capillary-assisted heat exchanger design and comparison with the existing design.

2. System description

The two-bed adsorption chiller employing silica gel-water pair, as described in our previous work [36], is considered for the entropy generation assessment. The heat and mass transfer models for entropy production have been incorporated into the numerically validated model presented in our previous work [36]. The schematic of the 10-kW two-bed adsorption testing unit is shown in Fig. 1. It has three auxiliary units; a heating water unit for the regeneration of the bed, a cooling water unit for adsorption and condensation, and a chilled water unit for generating the cooling effect. The flow of heating/cooling/chilled fluid is controlled by the operation of the motorized ball valves. The detailed working principle, experimental system layout, instrumentation and control, and valve operation have been summarized in Yagnamurthy et al. [36]. Table 1 shows the numerical values for input parameters used in the present computational study.

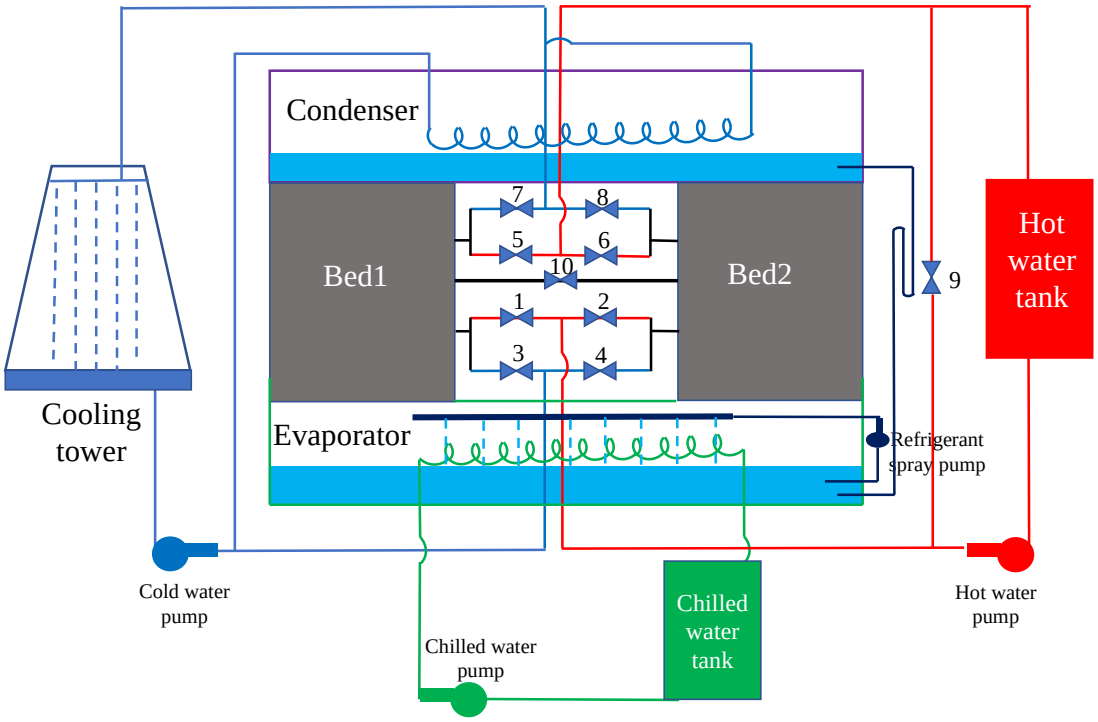

Fig. 1. Schematic of two-bed silica gel-water pair-based adsorption chiller.

Table 1. Values for parameters used in the present computation [36].

Parameter	Value	Unit
K_o	7.3×10^{-7}	Pa^{-1}
Q_{st}	2559	kJ/kg

x^*	0.4	kg/kg
D	6	-
D_o	2.54×10^{-4}	m^2/s
R_p	1.7×10^{-4}	M
E_a	42	kJ/mol
$\dot{m}_{hot/cool}$	0.80 (under rated condition)	kg/s
$\dot{m}_{chill}$	0.50 (under rated condition)	kg/s
$\dot{m}_{cond}$	0.63 (under rated condition)	kg/s
$(UA)_{bed}$	3.68	kW/K
$(MC_p)_{bed}$	68.38	kJ/K
$(UA)_{cond}$	8.55	kW/K
$(MC_p)_{cond}$	73.39	kJ/K
$(UA)_{evap}$	3.12	kW/K
$(MC_p)_{evap}$	337.55	kJ/K

3. Mathematical modelling

The mathematical modelling concerning the mass and energy balance for each component of the adsorption chiller during various processes has been carried out. The Second Law of Thermodynamics-based entropy generation analysis has also been carried out through suitable models for the heat and mass transfer processes across various components of the chiller along with the heat source and heat sink units.

3.1 Adsorption uptake

Tóth model (refer to Eq. (1)) is adapted to compute the equilibrium uptake, where the values of the respective parameters are given in Table 1.

$$x_{eq} = \frac{K_o P e^{(Q_{st}/RT)}}{\left[1+\left\{\frac{K_o P e^{(Q_{st}/RT)}}{x^*}\right\}^d\right]^{(1/d)}} \tag{1}$$

While presenting the interaction of adsorbate during the adsorption/desorption process, the Linear Driving Force (LDF) formulation is employed, as shown in Eq. (2).

$$\frac{dx}{dt} = 15\frac{D_o}{R_p^2}\left(x_{eq} - x\right) exp\left(-\frac{E_a}{RT}\right) \tag{2}$$

3.2 Energy balance in the heat exchangers

The first law of thermodynamics-based energy balance across the beds, condenser, and the evaporator is given by Eq. (3), Eq. (4), and Eq. (5), respectively. as described in our previous work [36].

$$\left[\left(Mc_p\right)_{hex} + \left(Mc_p\right)_{ads} + xM_{ads}c_{p,refrigerant}\right]\frac{dT_{bed}}{dt} - M_{ads}Q_{st}\frac{dx}{dt} = \dot{m}_{bed}c_{p,w}\left(T_{bed,in} - T_{bed,out}\right) = UA_{bed}LMTD_{bed} \quad (3)$$

$$\left[\left(Mc_p\right)_{cond}\right]\frac{dT_{cond}}{dt} + M_{ads}\left(\frac{dx}{dt}\right)_{des}\left[\left(h_{fg}\right)_{cond} + c_{p,vapour} \times \left(T_{des} - T_{cond}\right)\right] = \dot{m}_{cond}c_{p,w}\left(T_{cond,in} - T_{cond,out}\right) = UA_{cond}LMTD_{cond} \quad (4)$$

$$\left[\left(Mc_p\right)_{evap}\right]\frac{dT_{evap}}{dt} + M_{ads}\left(h_{fg}\right)_{evap}\left(\frac{dx}{dt}\right)_{ads} = \dot{m}_{chill}c_{p,w}\left(T_{chill/evap,in} - T_{chill/evap,out}\right) = UA_{evap}LMTD_{evap} \quad (5)$$

where the bed inlet temperature is computed assuming a linear relation with time for the first valve opening duration of 9 seconds, as shown in Eq. (6).

$$T_{bed,in} = T_{cool/hot,in} \times \frac{(t-\varphi)}{9} + T_{hot/cool,in} \times \frac{(9-t+\varphi)}{9} \quad (6)$$

3.3 Entropy generation assessment

The Second law of Thermodynamics quantifies energy destruction in terms of entropy and explains why entropy is always positive or constant for a closed system. Therefore, it can be a measure of a process's tendency to ensue in a specific direction and establishes the flow of energy in the form of heat from high-temperature to low-temperature regions.

3.3.1 Entropy generation in heat transfer

Heat transfer entropy generation for various components is estimated by dividing the heat exchanger tube into N segments and computing the entropy generation for each segment, as shown in Eq. (7), Eq. (8), Eq. (9), and Eq. (10).

$$S_{gen,HT,ads} = \frac{UA_{ads}}{N} \times \sum_{i=1}^{N}(T_i - T_{ads})\left[\frac{1}{T_{ads}} - \frac{1}{T_i}\right] \quad (7)$$

$$S_{gen,HT,des} = \frac{UA_{des}}{N} \times \sum_{i=1}^{N}(T_i - T_{des})\left[\frac{1}{T_{des}} - \frac{1}{T_i}\right] \quad (8)$$

$$S_{gen,HT,cond} = \frac{UA_{cond}}{N} \times \sum_{i=1}^{N}(T_i - T_{cond})\left[\frac{1}{T_{cond}} - \frac{1}{T_i}\right] \quad (9)$$

$$S_{gen,HT,evap} = \frac{UA_{evap}}{N} \times \sum_{i=1}^{N}\left(T_i - T_{evap}\right)\left[\frac{1}{T_{evap}} - \frac{1}{T_i}\right] \quad (10)$$

where $T_i = \frac{(T_{k,in} - T_{k,out})}{N} i + T_{k,out}$ and k can be *ads*, *des*, *cond*, or *evap* consequently.

3.3.2 Entropy generation in mass transfer

The entropy generation due to mass transfer in the adsorber, desorber, condenser, and evaporator components are computed using Eq. (11), Eq. (12), Eq. (13), and Eq. (14), respectively. For the mass transfer entropy generation across the adsorber, the refrigerant vapor is assumed to be in thermal equilibrium with the bed due to the negligible sensible heating fraction of the vapor in comparison to that of the bed.

$$S_{gen,MT,ads} = M_{bed} \left[\frac{dx}{dt}\right]_{ads} \left[\frac{Q_{st}}{T_{ads}} - \left(s_{g@T_{ads}} - s_{f@T_{ads}}\right)\right] \quad (11)$$

$$S_{gen,MT,des} = M_{bed} \left[\frac{dx}{dt}\right]_{des} \left[\frac{Q_{st}}{T_{des}} - \left(s_{g@T_{des}} - s_{f@T_{des}}\right)\right] \quad (12)$$

$$S_{gen,MT,cond} = M_{bed} \left[\frac{dx}{dt}\right]_{des} \left[\frac{h_{fg}}{T_{cond}} + c_{p,vapor} \ln\left(\frac{T_{des}}{T_{cond}}\right) - \left(s_{g@T_{des}} - s_{f@T_{cond}}\right)\right] \quad (13)$$

$$S_{gen,MT,evap} = M_{bed} \left[\frac{dx}{dt}\right]_{ads} \left[\frac{h_{fg}}{T_{evap}} - \left(s_{g@T_{evap}} - s_{f@T_{evap}}\right)\right] \quad (14)$$

3.3.3 Entropy generation in the heat source and heat sink

Apart from these, there is entropy generation occurring at the source (hot water tank) and sink (cooling tower), which is computed from Eq. (15) and Eq. (16), respectively.

$$S_{gen,HT\_sink} = \dot{m}_{flow} c_{p,water} \left[-\ln\left(\frac{T_{bed,out}}{T_{sink}}\right) + \frac{(T_{sink} - T_{bed,out})}{T_{sink}}\right] \quad (15)$$

$$S_{gen,HT\_source} = \dot{m}_{flow} c_{p,water} \left[\ln\left(\frac{T_{source}}{T_{bed,out}}\right) - \frac{(T_{source} - T_{bed,out})}{T_{source}}\right] \quad (16)$$

3.3.4 Total entropy generation in the system

The total entropy generation rate ($S_{gen,tot}$) is the summation of heat and mass transfer entropy generation rates across various components, as shown in Eq. (17).

$$S_{gen,tot} = S_{gen,ads} + S_{gen,des} + S_{gen,cond} + S_{gen,evap} + S_{gen,HT\_sink} + S_{gen,HT\_source} \quad (17)$$

where the entropy generation across a particular component '*k*' is shown in Eq. (18).

$$S_{gen,k} = S_{gen,HT,k} + S_{gen,MT,k} \quad (18)$$

where *k* can be *ads*/*des*/*cond*/*evap*.

3.3.5 Second law-based performance parameter: Specific irreversibility evaluation (X)

Apart from the cooling capacity and COP, the specific irreversibility, which is the irreversibility per unit cooling power output of the chiller, is evaluated in the present study as shown in Eq. (19).

$$X = \frac{T_{cool,in}\int_{t=o}^{cyc} S_{gen}dt}{\int_{t=o}^{cyc} m_{chill}\times 4.18\times(T_{chill,in}-T_{chill,out})dt} \quad (19)$$

Further, an efficiency parameter η is evaluated as a ratio of the system COP and Carnot COP for the given operating conditions, as shown in Eq. (20).

$$\eta = \frac{COP}{COP_{carnot}} \quad (20)$$

$$\text{where, } COP = \frac{\int_{t=o}^{cyc} m_{chill}\times 4.18\times(T_{chill,in}-T_{chill,out})dt}{\int_{t=o}^{cyc} m_{hot}\times 4.18\times(T_{hot,in}-T_{hot,out})dt} \quad (21)$$

$$COP_{carnot} = \left(1-\frac{T_{cool,in}}{T_{hot,in}}\right)\left(\frac{T_{chill,in}}{T_{cool,in}-T_{chill,in}}\right) \quad (22)$$

4. Results and Discussion

In order to validate the numerical model, the experimental values of various inlet temperatures, including hot water, cooling water, and chilled water are utilized as the input parameters. The profiles of outlet temperatures throughout a half-cycle for different components of the chiller show the same pattern for both numerical and experimental outcomes as shown in Fig. 2.

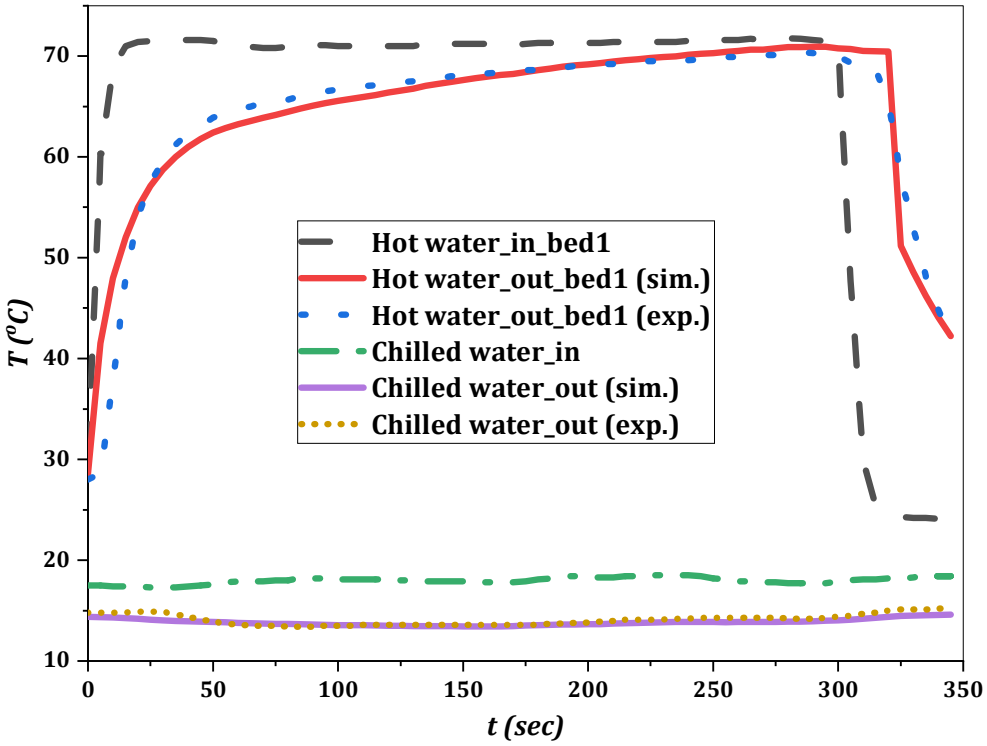

(a)

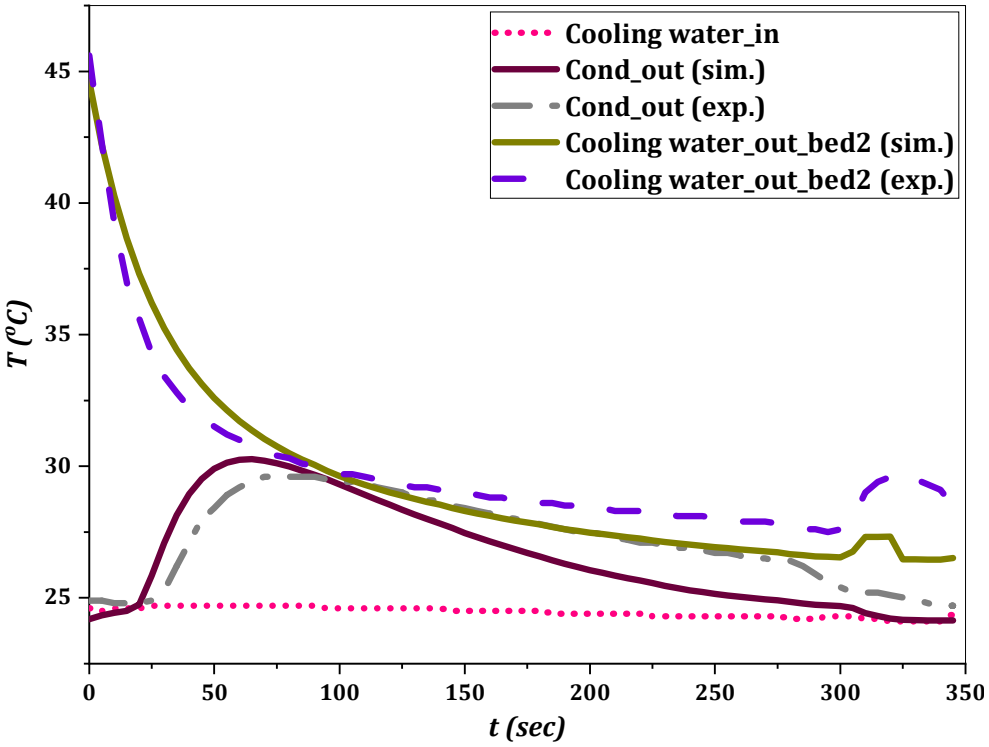

(b)

Fig. 2. Experimental versus numerical profiles for various outlet temperatures.

The normalised root mean squared errors between the numerically and experimentally estimated outlet temperatures of water streams for bed 1, bed 2, condenser, and evaporator are found to be 6.8%, 4.2%, 4.1%, and 2.6%, respectively. Therefore, it can be summarized that the proposed numerical modelling is found to be in good agreement with the experimental outcomes. The entropy generation for various phases of the operating cycle is discussed in the subsequent sections.

4.1 Entropy generation during normal operation

The present computational effort aims to comprehend the irreversibilities in terms of entropy production caused by temperature inadequacy inside the various components and processes, as well as within the heat reservoirs such as cooling towers and hot water tanks. The variation of the entropy generation rate over the half-cycle duration of a normal operation is shown in Fig. 3. The entropy generation caused by heat transfer in the adsorber component is the dominating component. The heat transfer entropy in the adsorber bed has a steep rise initially during the valve opening duration due to the sudden influx of cooling water and vice-versa for the desorber bed. The heat transfer

entropy generation of the adsorbing bed gradually reduces over the adsorption cycle as the bed temperature approaches that of the cooling water inlet. For the desorbing bed, on the other hand, the entropy generation rate increases initially due to the flushing of the trapped cooling water and reduces eventually as the temperature of the desorbing bed approaches that of the inlet hot water temperature. The entropy shoot-up at the beginning of the switch-over phase, where the cooling water enters the desorbed bed, flushing out the trapped hot water, as explained in our previous study [36]. Further, the entropy generation caused by mass transfer is seen to be significantly lower than that of heat transfer, implying that the entropy change due to phase change is not as significant as that of the entropy generation arising out of temperature differences. The mass transfer entropy generation rate is seen to be the highest for the condensation process, as it involves the de-superheating of the desorbed vapor along with the phase change process, which sets it apart from the other components. The mass transfer entropy generation rate follows the trend of the adsorption/desorption rates, which increase initially with the change in bed temperature and eventually reduce as the beds approach saturation.

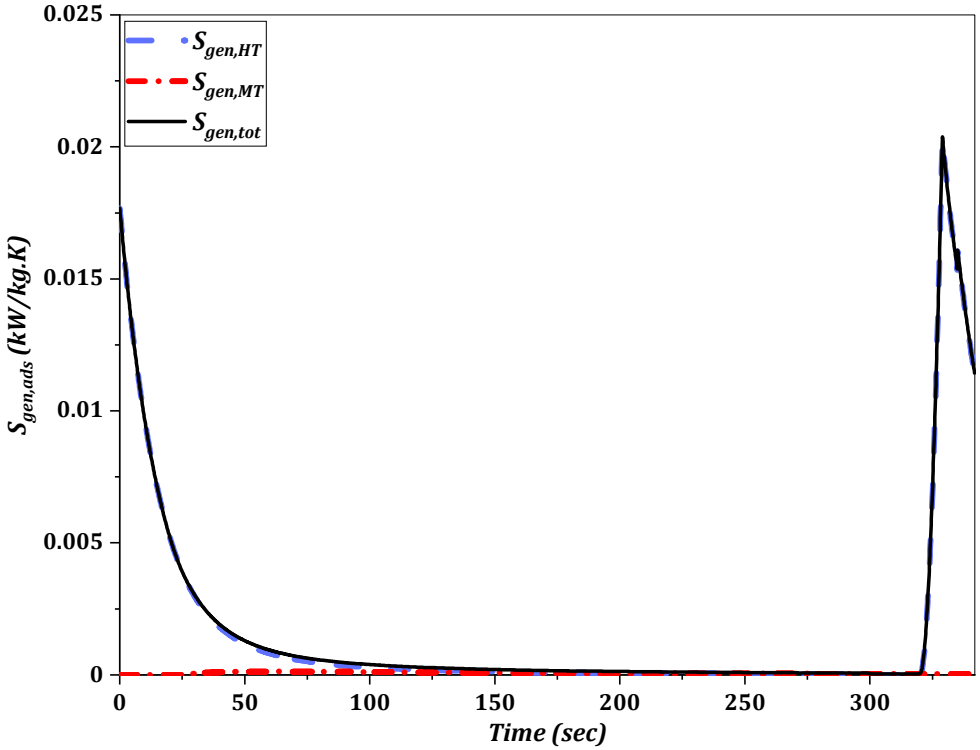

(a)

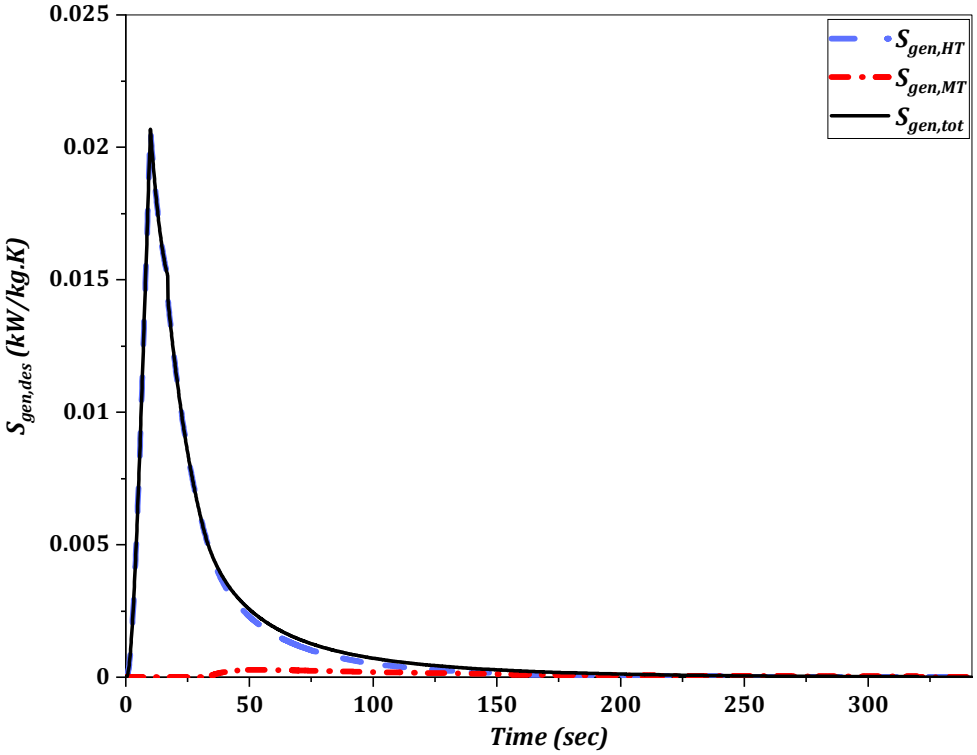
0.025
0.02
0.015
0.01
0.005
0
0
50
100
150
200
250
300
$S_{gen,des}$ (kW/kg.K)
Time (sec)
$S_{gen,HT}$
$S_{gen,MT}$
$S_{gen,tot}$

(b)

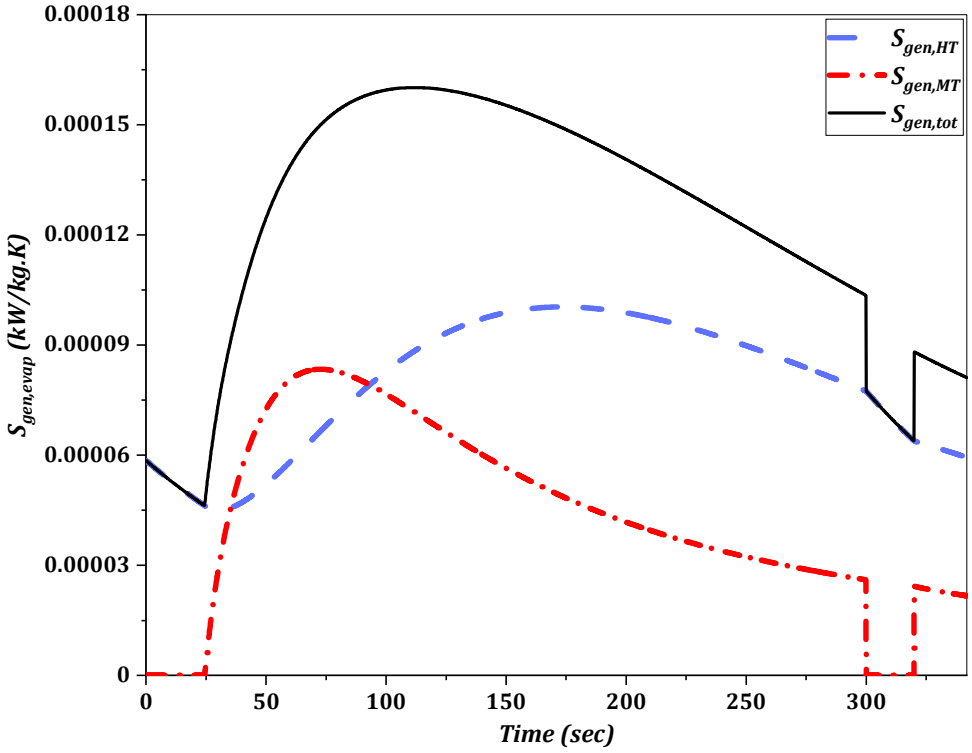
0.00018
0.00015
0.00012
0.00009
0.00006
0.00003
0
0
50
100
150
200
250
300
$S_{gen,evap}$ (kW/kg.K)
Time (sec)
$S_{gen,HT}$
$S_{gen,MT}$
$S_{gen,tot}$

(c)

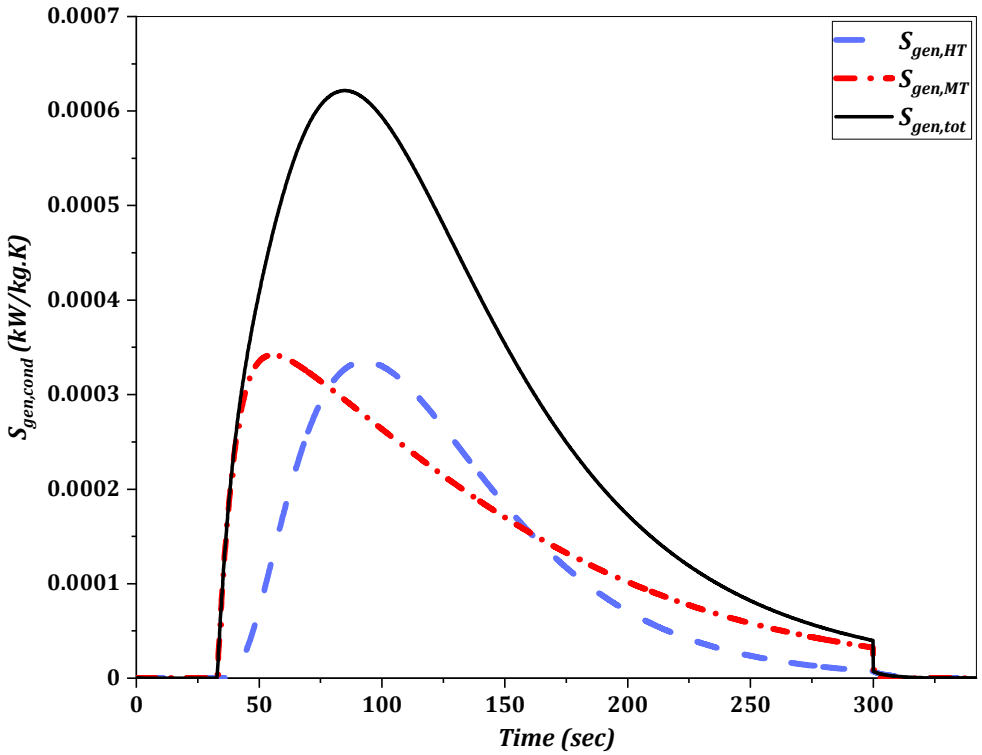

(d)

Fig. 3. Entropy generation during adsorption (a); desorption (b); evaporation (c); and condensation (d) with normal operation.

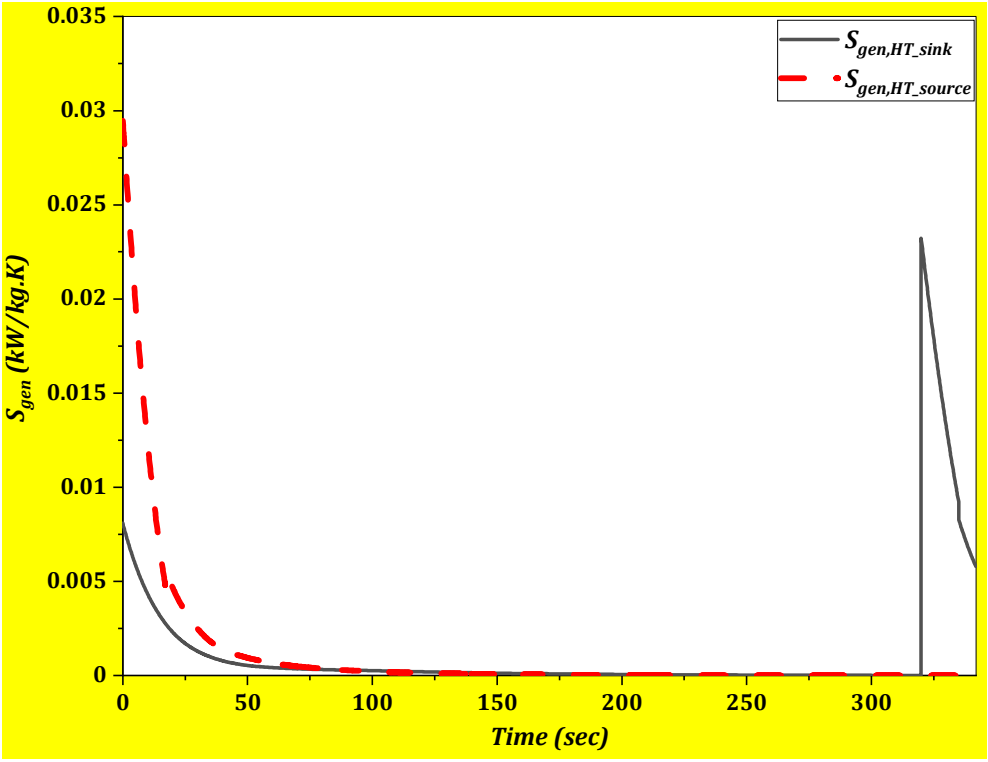

Fig. 4. Entropy generation in heat sink and heat source during normal operation.

From Fig. 4, it can be seen that the numerical profiles of entropy generation over the period inside the cooling tower or heat sink and hot water tank or heat source have a steep rise at the beginning of the half-cycle and then gradually decrease as the outlet temperatures of the hot and cooling water streams approach that of the respective inlet temperatures. The presence of high-temperature thermal energy generates a huge amount of irreversibility at the beginning of the half-cycle in the hot water tank as the trapped cooling water in the adsorber tube enters it. Similarly, a spike in the entropy generation value is observed in the heat sink towards the end of the half-cycle due to the hot water entry into the cooling tower at the beginning of the switch-over phase, as explained in Yagnamurthy et al. [36].

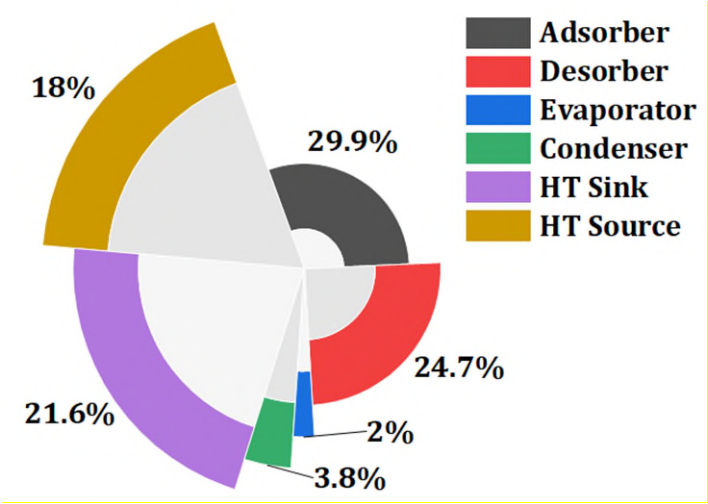

Fig. 5. Percentage contribution in entropy generation by various components during normal operation.

Fig. 5 illustrates the percentage contribution in the total entropy generation by various components over a half cycle. The total entropy production at the adsorber occupies the major share, followed by the desorber, heat sink, heat source, condenser, and evaporator. The cooling water flows to the desorbed bed during the switch over phase of the half cycle along with the adsorbing bed to ensure a longer adsorption time as explained in our previous work [36]. This results in a marginal increase in the entropy generation during adsorption over that of desorption. The heat sink entropy generation is due to the streams from the adsorber bed as well as the condenser, thus causing it to have a slightly higher entropy generation value over that of the heat source. It can be inferred that the beds are crucial to the entropy generation followed by the heat source and sink. The heat transfer enhancement in the adsorbent bed can be accomplished through heat exchanger

design modifications such as having a better adsorbent-to-metal mass ratio, better heat transfer coefficient, etc. The entropy generation at the heat source and sinks, on the other hand, can be minimized by implementing various recovery mechanisms without needing to modify the system design, one of which is addressed in the following subsection.

4.2 Entropy generation during passive heat recovery

The passive heat recovery operation involves heat recovery from the water trapped in the heat exchanger tubes and a portion of the desorbed bed's thermal energy through the diversion of the outlet streams of hot and cooling water to their alternate destinations, as described in our previous work [36]. On employing the passive heat recovery technique, the curves for heat transfer and mass transfer entropy generation across the adsorber and the desorber have essentially identical behavior throughout the cycle, as depicted in Fig 6. A sudden surge in the heat transfer entropy generation is observed towards the end of the half-cycle, where the cross-over operation of the water streams takes place and the flushing of trapped water streams commences. The entropy generation occurring in the adsorption beds remains dominant, as seen with normal operation. The mass transfer entropy generation is also seen to be the highest for the condensation process similar to that of normal operation.

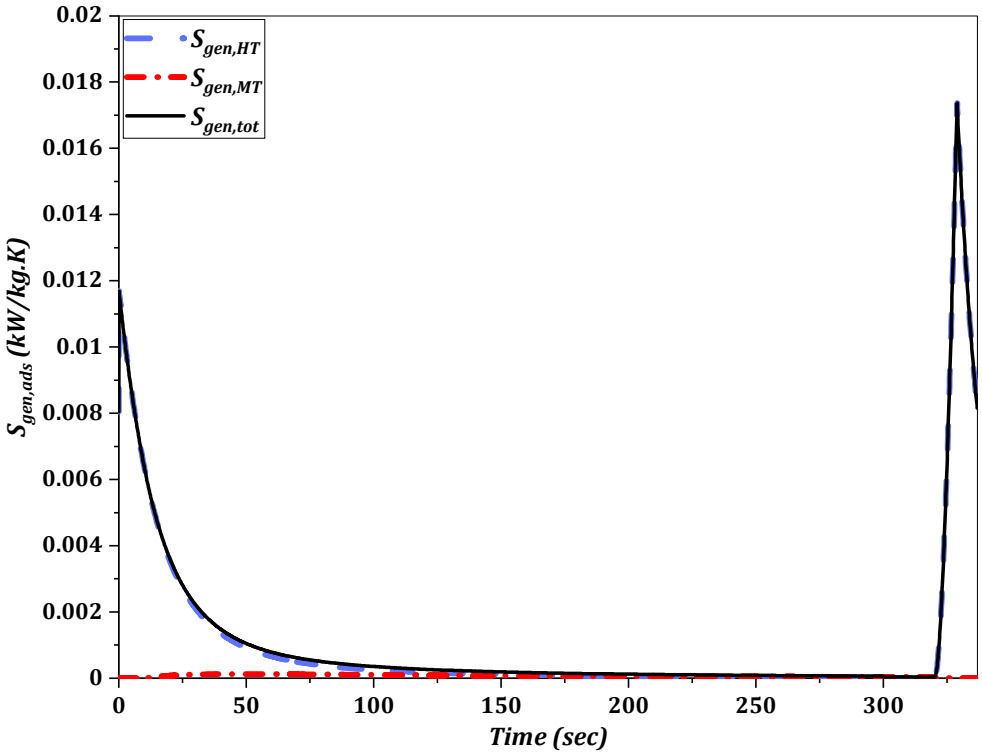

(a)

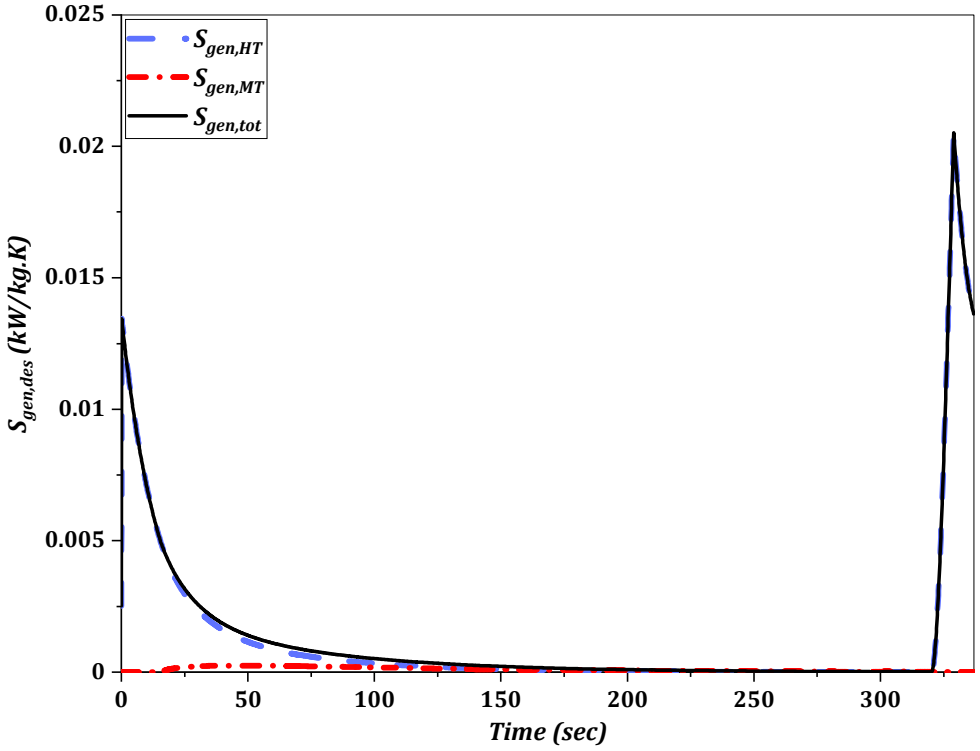
0.025
0.02
0.015
0.01
0.005
0
0
50
100
150
200
250
300
$S_{gen,des}$ (kW/kg.K)
Time (sec)
$S_{gen,HT}$
$S_{gen,MT}$
$S_{gen,tot}$

(b)

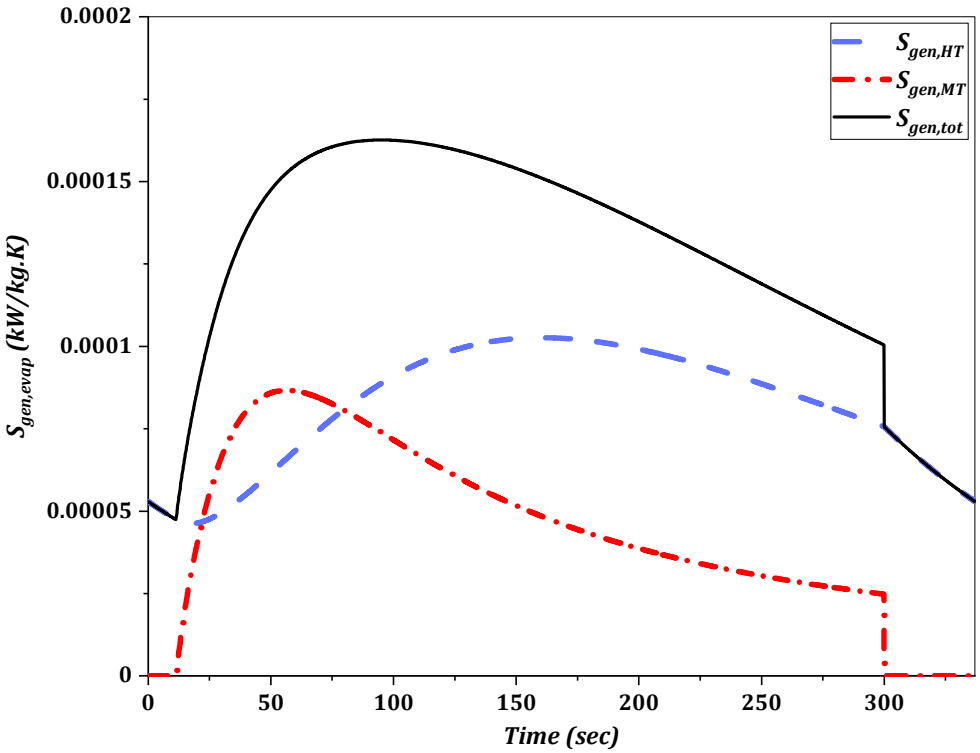
0.0002
0.00015
0.0001
0.00005
0
0
50
100
150
200
250
300
$S_{gen,evap}$ (kW/kg.K)
Time (sec)
$S_{gen,HT}$
$S_{gen,MT}$
$S_{gen,tot}$

(c)

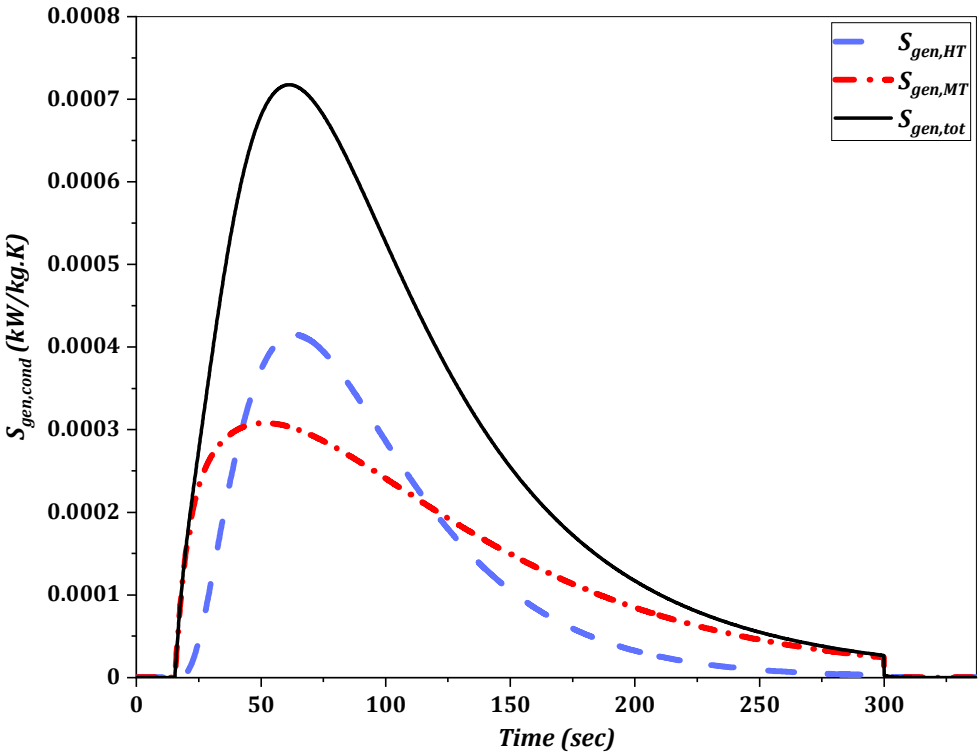

(d)

Fig. 6. Entropy generation during adsorption (a); desorption (b); evaporation (c); and condensation (d) with passive heat recovery scheme.

The entropy generation contributed in the chiller unit at the heat source and sinks, heat transfer, and mass transfer during the passive heat recovery mechanism is shown in Fig. 7. It can be seen that entropy generation follows a similar trend for both the heat source and heat sink, with a surge towards the end of the half-cycle due to the commencement of the passive heat recovery operation involving the flushing of beds. The entropy generation is seen to be higher for the heat sink due to a slightly higher temperature difference between the cooling tower water inlet and outlet streams in comparison to that of the hot water tank at the end of the cross-over operation of the passive heat recovery strategy. This can be attributed to the tube and valve arrangement and the selected flow rate values of various streams for the operation of the chiller.

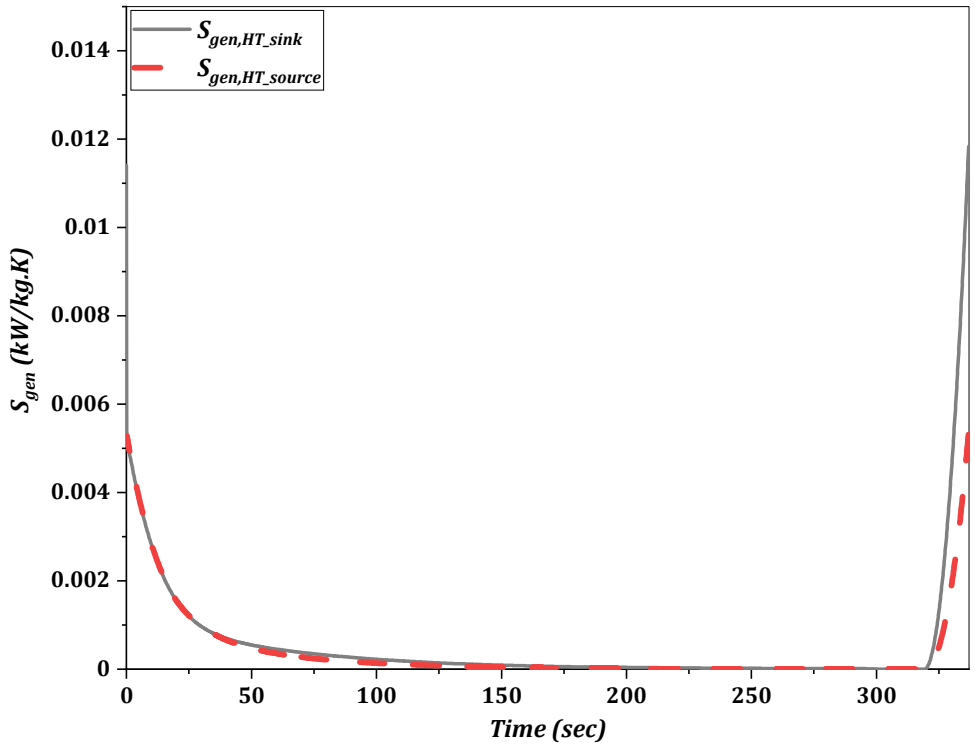
S_{gen,HT_sink}
S_{gen,HT_source}
S_{gen} (kW/kg.K)
0.014
0.012
0.01
0.008
0.006
0.004
0.002
0
0
50
100
150
200
250
300
Time (sec)

(a)

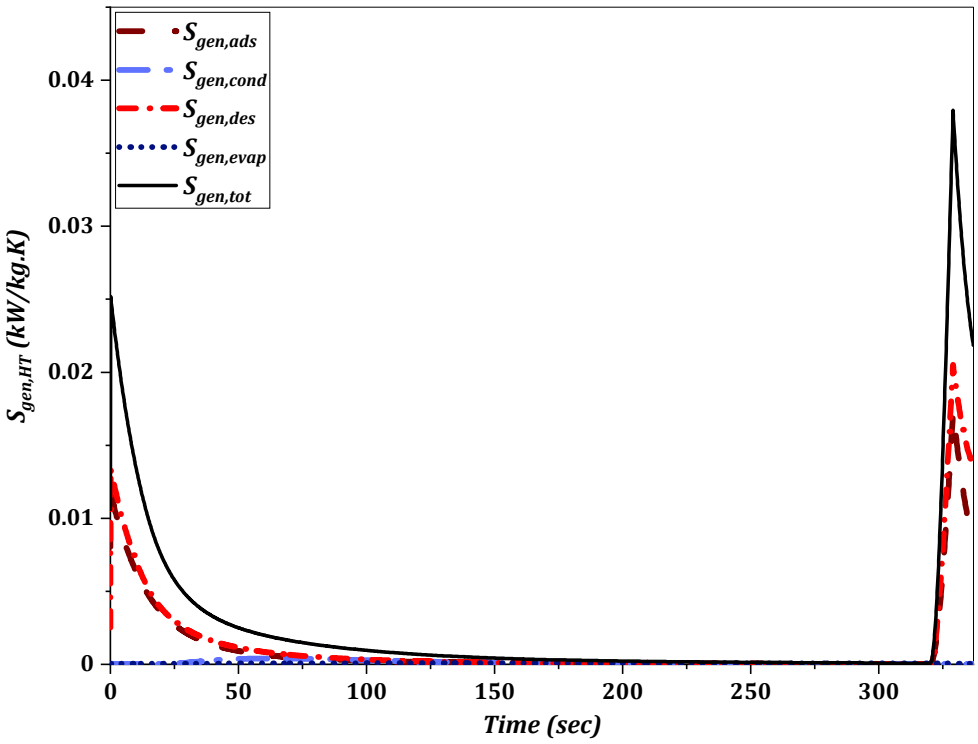
$S_{gen,ads}$
$S_{gen,cond}$
$S_{gen,des}$
$S_{gen,evap}$
$S_{gen,tot}$
$S_{gen,HT}$ (kW/kg.K)
0.04
0.03
0.02
0.01
0
0
50
100
150
200
250
300
Time (sec)

(b)

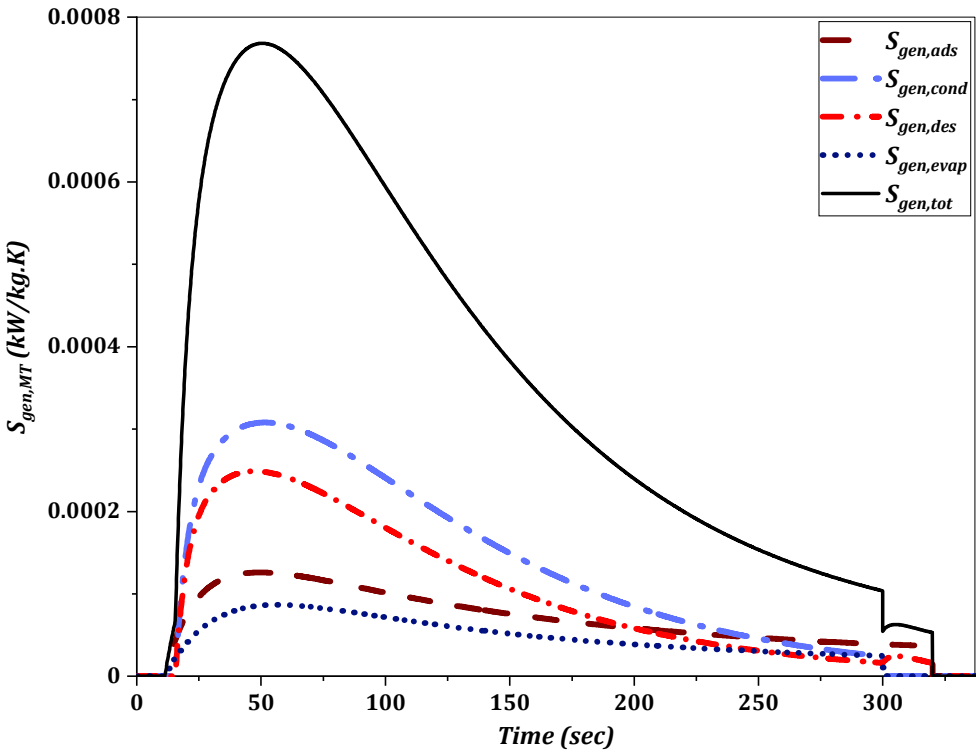

(c)

Fig. 7. Entropy generation in heat sink and heat source (a); heat transfer (b); and mass transfer (c) with passive heat recovery scheme.

4.3 Normal operation versus passive heat recovery

This section addresses the irreversibility reduction potential of the passive heat recovery strategy against the normal operation of the adsorption chiller. The combined total of heat and mass transfer entropies generated over a half cycle among various components and processes of the chiller is shown in Fig. 8 for both normal and passive heat recovery operations. It is observed that there is a slight reduction in the entropy generation during the adsorption process with the passive heat recovery strategy in comparison to that of the normal operation. This can be attributed to the relatively long duration of the adsorption process due to the switch-over phase in the normal operation in comparison to that of the passive heat recovery operation.

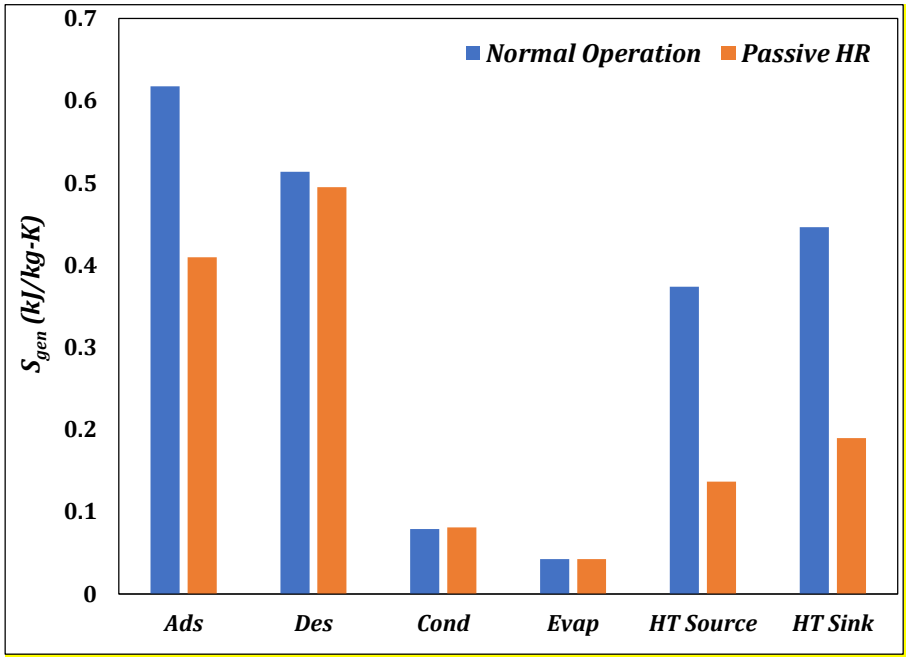

Fig. 8. Total entropy generation in various components over a half cycle.

The desorption, evaporation, and condensation processes can be seen to have nearly equal entropy generation rates for both operations, owing to their similarities. The entropy generation at the heat source and heat sink can be seen to be significantly reduced with the passive heat recovery strategy due to the reduction of mixing losses of water streams of large temperature differences occurring at the end of every half cycle in a normal operation. The percentage reductions in entropy generation by passive heat recovery strategy are estimated as 33.63%, 63.41%, and 57.49% for adsorption, heat source, and heat sink, respectively, over that of the normal operation.

4.4 Optimal operating temperature identification

The irreversibility per unit of cooling energy generated for both the normal and passive heat recovery operations is shown in Fig. 9 for various hot water inlet temperatures. The specific irreversibility first decreases and then increases as the hot water temperature increases from 55 to 90 ^{o}C. This can be attributed to the lower cooling energy output at lower hot water inlet temperatures and higher irreversibility at higher hot water inlet temperatures.

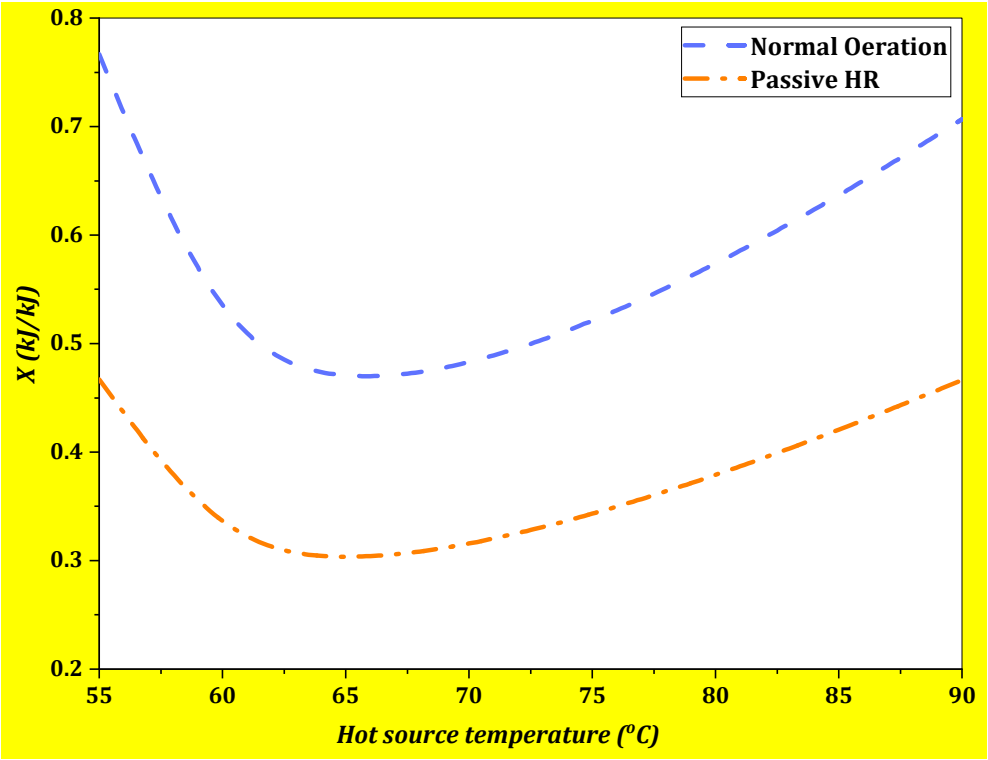

Fig. 9. Specific irreversibility variation with hot water inlet temperature.

The minimum value of specific irreversibility is seen to be at 65°C for both the normal and passive heat recovery operations. The specific irreversibility impact on the second law efficiency is reflected in the efficiency parameter trends shown in Fig. 10 for various hot water inlet temperatures. It can be seen that the efficiency parameter's value increases with decreasing specific irreversibility, implying that the system COP reaches closer to that of its Carnot COP. The maximum value of η is also seen to be at 65°C. It can thus be concluded the heat captured at this temperature from the heat source is utilized the most effectively to produce the desired effect with the present chiller. This finding can be particularly useful for deciding the effective waste heat recovery technologies for a given hot source temperature. It can also be observed that the passive heat recovery operation yields lower X and higher η values at all the hot water inlet temperatures, owing to its lower entropy generation. While the minimum specific irreversibility for the normal operation is found to be 0.46 kJ/kJ, that of the passive heat recovery operation is seen to reduce by over 35% amounting to 0.30 kJ/kJ. The improvement in η on the other hand is seen to be 34%. Thus, the passive heat recovery mode can be said to be better over the default mode, from the perspective of both the first and second thermodynamic laws.

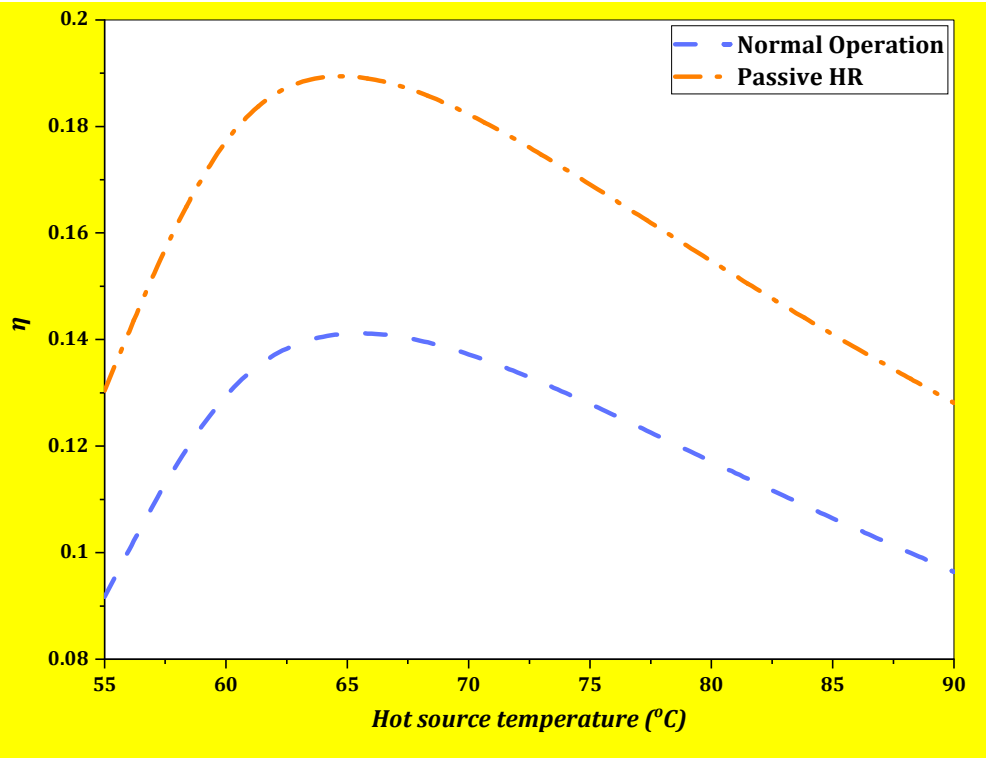

Fig. 10. Efficiency parameter variation with hot water inlet temperatures.

4.5. Comparison with the capillary-assisted evaporator

The chiller has a total auxiliary electric power consumption of 1.3 kW, out of which the evaporator spray pump has a power consumption of around 100 W. This electric power consumption of 100 W can be a direct saving with the capillary assisted-evaporator design. Since electricity is a high-grade energy source, the electricity consumption of the evaporator spray pump can be directly incorporated into the specific irreversibility evaluation for comparison with that of the capillary-assisted evaporator design, as shown in Eq. (23) and Eq. (24). A capillary assisted evaporator taken from Pialago et al. [38] is seen to be suitable for the present chiller and has been scaled up to match the present evaporator's heat capacity. The heat capacity (C_p) and overall heat transfer coefficient (UA) values of the capillary-assisted heat exchanger are 337.5 kJ/K and 2.38 kW/K, respectively.

$$X_{spray\ pump} = \frac{T_{cool,in}\int_{t=o}^{cyc} S_{gen}dt + 0.1\int_{t=o}^{cyc} dt}{\int_{t=o}^{cyc} m_{chill}\times 4.18\times(T_{chill,in}-T_{chill,out})dt} \quad (23)$$

$$X_{capillary} = \frac{T_{cool,in}\int_{t=o}^{cyc} S_{gen}dt}{\int_{t=o}^{cyc} m_{chill}\times 4.18\times(T_{chill,in}-T_{chill,out})dt} \quad (24)$$

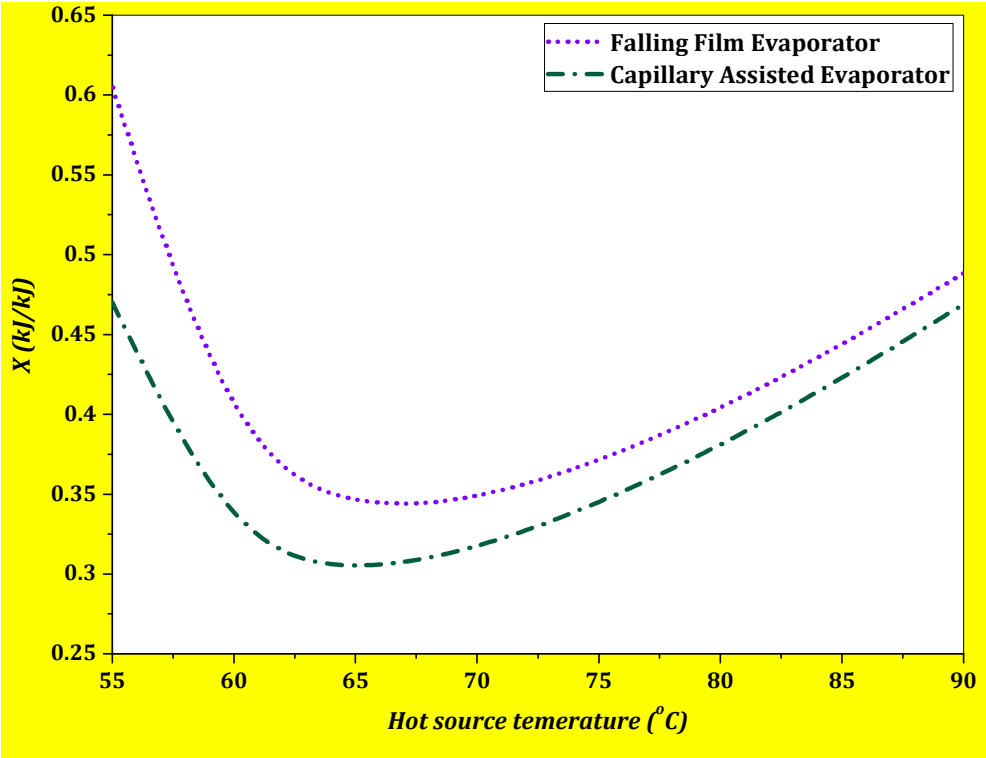

Fig. 11. Specific irreversibility variation with hot water inlet temperature.

Fig. 11 shows the comparison between the specific irreversibility values between the two evaporator designs with a passive heat recovery operation. It can be seen that a capillary assisted-evaporator design yields lower specific irreversibility generation by up to 22%, mainly resulting from the savings in the electrical energy.

5. Conclusions

Entropy generation has been evaluated for various components of a two-bed silica gel-water adsorption chiller, along with those occurring at the heat source and sink. The second law analysis has been extended for a passive heat recovery operational mode along with a normal operational mode, in the present study. The highest entropy generation is found to be occurring at the adsorber followed by the desorber, heat sink, heat source, condenser, and evaporator, respectively for both the operating strategies. An entropy generation reduction of up to 63% is seen with the passive heat recovery mode over that of the default operating mode. Further, the specific irreversibility evaluation has been presented as an indicator of second law efficiency to determine the optimum operating conditions. A hot water inlet temperature of 65°C is identified as the optimum temperature for the most effective heat utilization and the passive heat recovery operation is seen to reduce the specific irreversibility by 35%. Finally, incorporating a

capillary-assisted evaporator is seen to be effective for further reducing specific irreversibility by up to 22% with the reduction of auxiliary electric power consumption. The present study's findings aimed to facilitate the effective use of waste heat for adsorption-based cooling applications and further the scope of capillary-assisted evaporators for adsorption cooling systems.

CRediT authorship contribution statement

P. R. Chauhan: Conceptualization, Investigation, Methodology, Writing - original draft. **S. Yagnamurthy:** Data collection, Validation, Writing - original draft. **B. B. Saha:** Supervision, Writing - review & editing. **S. K. Tyagi:** Conceptualization, Supervision, Writing - review & editing.

Declaration of competing interest

The authors declare that they have no known competing financial interests or personal relationships that could have appeared to influence the work reported in this paper.

Acknowledgments

One of the authors (PRC) thankfully acknowledges the financial assistance in the form of fellowship due to the Department of Energy Science and Engineering, Indian Institute of Technology Delhi. The authors are also thankful to the learned reviewers and the Editor for providing the fruitful suggestions, to modify the manuscript into the present form.

References

[1] Saren, S., Mishra, V. K., Thu, K., & Mitra, S. (2022). Scaling analysis of large pressure jump driven adsorption of water vapour in columnar porous silica gel bed. *International Communications in Heat and Mass Transfer*, *135*, 106101.

[2] Wan, A., Yang, J., Chen, T., & Huang, J. (2021). Techno-economic analysis of combined cycle power plant with waste heat-driven adsorption inlet air cooling system. *International Communications in Heat and Mass Transfer*, *126*, 105422.

[3] Yagnamurthy, S., Rakshit, D., Jain, S., Rocky, K. A., Islam, M. A., & Saha, B. B. (2021). Adsorption of difluoromethane onto activated carbon based composites: Thermophysical properties and adsorption characterization. *International Journal of Heat and Mass Transfer*, *171*, 121112.

[4] Chauhan, P. R., Kaushik, S. C., & Tyagi, S. K. (2022). A review on thermal performance enhancement of green cooling system using different adsorbent/refrigerant pairs. *Energy Conversion and Management: X*, 100225.

[5] Rocky, K. A., Pal, A., Rupam, T. H., & Saha, B. B. (2021). Zeolite-graphene composite adsorbents for next generation adsorption heat pumps. *Microporous and Mesoporous Materials*, *313*, 110839.

[6] Raymond, A., & Garimella, S. (2021). A theoretical treatment of the design and optimization of adsorption heat pumps. *Applied Thermal Engineering*, *184*, 116305.

[7] Chauhan, P. R., Kaushik, S. C., & Tyagi, S. K. (2022). Current status and technological advancements in adsorption refrigeration systems: A review. *Renewable and Sustainable Energy Reviews*, *154*, 111808.

[8] Aristov, Y. I. (2021). Adsorptive conversion of ultralow-temperature heat: Thermodynamic issues. *Energy*, *236*, 121892.

[9] Rupam, T. H., Palash, M. L., Islam, M. A., & Saha, B. B. (2022). Transitional metal-doped aluminum fumarates for ultra-low heat driven adsorption cooling systems. *Energy*, *238*, 122079.

[10] Bilal, M., Sultan, M., Morosuk, T., Den, W., Sajjad, U., Aslam, M. M., ... & Farooq, M. (2022). Adsorption-based atmospheric water harvesting: A review of adsorbents and systems. *International Communications in Heat and Mass Transfer*, *133*, 105961.

[11] Zendehboudi, A., Angrisani, G., & Li, X. (2018). Parametric studies of silica gel and molecular sieve desiccant wheels: Experimental and modeling approaches. *International Communications in Heat and Mass Transfer*, 91, 176-186.

[12] Shoeibi, S., Saemian, M., Kargarsharifabad, H., Hosseinzade, S., Rahbar, N., Khiadani, M., & Rashidi, M. M. (2022). A review on evaporation improvement of solar still desalination using porous material. *International Communications in Heat and Mass Transfer*, 138, 106387.

[13] Demir, H., Mobedi, M., & Ülkü, S. (2009). Effects of porosity on heat and mass transfer in a granular adsorbent bed. *International Communications in Heat and Mass Transfer*, 36(4), 372-377.

[14] Ilis, G. G., Mobedi, M., & Ülkü, S. (2010). A parametric study on isobaric adsorption process in a closed adsorbent bed. *International communications in heat and mass transfer*, 37(5), 540-547.

[15] Pahinkar, D. G., Boman, D. B., & Garimella, S. (2020). High performance microchannel adsorption heat pumps. *International Journal of Refrigeration*, 119, 184-194.

[16] Dias, J. M., & Costa, V. A. (2020). Evaluating the performance of a coated tube adsorber for adsorption cooling. *International Journal of Refrigeration*, 118, 21-30.

[17] Pahinkar, D. G., Boman, D. B., & Garimella, S. (2020). High performance microchannel adsorption heat pumps. *International Journal of Refrigeration*, 119, 184-194.

[18] Farid, S. K., Billah, M. M., Khan, M. Z. I., Rahman, M. M., & Sharif, U. M. (2011). A numerical analysis of cooling water temperature of two-stage adsorption chiller along with different mass ratios. *International Communications in Heat and Mass Transfer*, 38(8), 1086-1092.

[19] Muttakin, M., Islam, M. A., Malik, K. S., Pahwa, D., & Saha, B. B. (2021). Study on optimized adsorption chiller employing various heat and mass recovery schemes. *International Journal of Refrigeration*, 126, 222-237.

[20] Riaz, N., Sultan, M., Miyazaki, T., Shahzad, M. W., Farooq, M., Sajjad, U., & Niaz, Y. (2021). A review of recent advances in adsorption desalination technologies. *International Communications in Heat and Mass Transfer*, 128, 105594.

[21] Thu, K., Kim, Y. D., Myat, A., Chun, W. G., & Ng, K. C. (2013). Entropy generation analysis of an adsorption cooling cycle. *International Journal of Heat and Mass Transfer*, *60*, 143-155.

[22] Sciacovelli, A., Verda, V., & Sciubba, E. (2015). Entropy generation analysis as a design tool—A review. *Renewable and Sustainable Energy Reviews*, *43*, 1167-1181.

[23] Bejan, A. (1977). The concept of irreversibility in heat exchanger design. *Trans ASME*, *99*, 374- 380.

[24] Meunier, F., Kaushik, S. C., Neveu, P., & Poyelle, F. (1996). A comparative thermodynamic study of sorption systems: second law analysis. *International Journal of Refrigeration*, *19*(6), 414-421.

[25] Meunier, F., Poyelle, F., & LeVan, M. D. (1997). Second-law analysis of adsorptive refrigeration cycles: the role of thermal coupling entropy production. *Applied Thermal Engineering*, *17*(1), 43-55.

[26] Pons, M. (1997). Analysis of the adsorption cycles with thermal regeneration based on the entropic mean temperatures. *Applied Thermal Engineering*, *17*(7), 615-627.

[27] Meunier, F. (1985). Second law analysis of a solid adsorption heat pump operating on reversible cascade cycles: application to the zeolite-water pair. *Journal of heat recovery systems*, *5*(2), 133-141.

[28] Pons, M. (1996). Second law analysis of adsorption cycles with thermal regeneration. *Journal of Energy Resources Technology, 118(3),* 229-236.

[29] Chua, H. T., Ng, K. C., Malek, A., & Oo, N. M. (2001). General thermodynamic framework for understanding temperature-entropy diagram of batchwise operating thermodynamic cooling cycles. *Journal of Applied Physics*, *89*(9), 5151-5158.

[30] Chua, H. T., Gordon, J. M., Ng, K. C., & Han, Q. (1997). Entropy production analysis and experimental confirmation of absorption systems. *International journal of refrigeration*, *20*(3), 179-190.

[31] Chua, H. T., Ng, K. C., Malek, A., Kashiwagi, T., Akisawa, A., & Saha, B. B. (1998). Entropy generation analysis of two-bed, silica gel-water, non-regenerative adsorption chillers. *Journal of Physics D: Applied Physics*, *31*(12), 1471.

[32] Myat, A., Thu, K., Ng, K. C., & Kim, Y. D. (2012). An entropy generation and genetic algorithm optimization of two-bed adsorption cooling cycle. *Proceedings of the Institution of Mechanical Engineers, Part E: Journal of Process Mechanical Engineering*, *226*(2), 142-156.

[33] Gado, M. G., Ookawara, S., Nada, S., & Hassan, H. (2022). Renewable energy-based cascade adsorption-compression refrigeration system: Energy, exergy, exergoeconomic and enviroeconomic perspectives. *Energy*, *253*, 124127. https://www.sciencedirect.com/science/article/abs/pii/S0735193321004875

[34] Hassan, A. A., Elwardany, A. E., Ookawara, S., Sekiguchi, H., & Hassan, H. (2022). Energy, exergy, economic and environmental (4E) assessment of hybrid solar system powering adsorption-parallel/series ORC multigeneration system. *Process Safety and Environmental Protection*.

[35] Alsarayreh, A. A., Al-Maaitah, A., Attarakih, M., & Bart, H. J. (2021). Energy and Exergy Analyses of Adsorption Chiller at Various Recooling-Water and Dead-State Temperatures. *Energies*, *14*(8), 2172.

[36] Yagnamurthy, S., Rakshit, D., Jain, S., & Saha, B. B. (2021). Operational envelope and performance enhancement of a two-bed adsorption cooling system. *Applied Thermal Engineering*, 117181.

[37] Lanzerath, F., Seiler, J., Erdogan, M., Schreiber, H., Steinhilber, M., & Bardow, A. (2016). The impact of filling level resolved: Capillary-assisted evaporation of water for adsorption heat pumps. *Applied Thermal Engineering*, *102*, 513-519.

[38] Pialago, E. J. T., Yoo, J., Zheng, X., Kim, B. R., Hong, S. J., Kwon, O. K., & Park, C. W. (2020). Experimental investigation of the heat transfer performance of capillary-assisted horizontal evaporator tubes with sintered porous hydrophilic copper-carbon nanotube-titanium dioxide (Cu-CNT-TiO2) composite coatings for adsorption chiller. *International Journal of Heat and Mass Transfer*, 147, 118958.

[39] Seiler, J., Lanzerath, F., Jansen, C., & Bardow, A. (2019). Only a wet tube is a good tube: Understanding capillary-assisted thin-film evaporation of water for adsorption chillers. *Applied Thermal Engineering*, *147*, 571-578.

[40] Thimmaiah, P. C., Sharafian, A., Huttema, W., McCague, C., & Bahrami, M. (2016). Effects of capillary-assisted tubes with different fin geometries on the performance of a low-operating pressure evaporator for adsorption cooling system applications. *Applied Energy*, *171*, 256-265.

[41] Thimmaiah, P. C., Sharafian, A., Huttema, W., Osterman, C., Ismail, A., Dhillon, A., & Bahrami, M. (2016). Performance of finned tubes used in low-pressure capillary-assisted evaporator of adsorption cooling system. *Applied Thermal Engineering*, *106*, 371-380.